

Article

The Generation of Equal-Intensity and Multi-Focus Optical Vortices by a Composite Spiral Zone Plate

Huaping Zang¹, Jingzhe Li¹, Chenglong Zheng^{1,*}, Yongzhi Tian¹, Lai Wei², Quanping Fan², Shaoyi Wang², Chuanke Wang², Juan Xie^{1,*} and Leifeng Cao³

¹ Key Laboratory of Materials Physics, Ministry of Education, School of Physics, Zhengzhou University, Zhengzhou 450001, China; zanghuaping@zzu.edu.cn (H.Z.); ljingzhe@gs.zzu.edu.cn (J.L.); yztian@zzu.edu.cn (Y.T.)

² Nation Key Laboratory of Plasma Physics, Laser Fusion Research Center, China Academy of Engineering Physics, Mianyang 621900, China; future718@yeah.net (L.W.); fanquanping@sina.cn (Q.F.); cslr1113@163.com (S.W.); wck1981@caep.cn (C.W.)

³ School of Engineering Physics, Shenzhen Technology University, Shenzhen 518118, China; caoleifeng@sztu.edu.cn

* Correspondence: clzheng@zzu.edu.cn (C.Z.); juanxie@zzu.edu.cn (J.X.)

Abstract: We propose a new vortex lens for producing multiple focused coaxial vortices with approximately equal intensities along the optical axis, termed equal-intensity multi-focus composite spiral zone plates (EMCSZPs). In this typical methodology, two concentric conventional spiral zone plates (SZPs) of different focal lengths were composited together and the alternate transparent and opaque zones were arranged with specific m-bonacci sequence. Based on the Fresnel–Kirchhoff diffraction theory, the focusing properties of the EMCSZPs were calculated in detail and the corresponding demonstration experiment was been carried out to verify our proposal. The investigations indicate that the EMCSZPs indeed exhibit superior performance, which accords well with our physical design. In addition, the topological charges (TCs) of the multi-focus vortices can be flexibly selected and controlled by optimizing the parameters of the zone plates. These findings which were demonstrated by the performed experiment may open new avenues towards improving the performance of biomedical imaging, quantum computation and optical manipulation.



Citation: Zang, H.; Li, J.; Zheng, C.; Tian, Y.; Wei, L.; Fan, Q.; Wang, S.; Wang, C.; Xie, J.; Cao, L. The

Generation of Equal-Intensity and Multi-Focus Optical Vortices by a Composite Spiral Zone Plate.

Photonics **2024**, *11*, 466. <https://doi.org/10.3390/photonics11050466>

Received: 27 March 2024

Revised: 2 May 2024

Accepted: 10 May 2024

Published: 15 May 2024



Copyright: © 2024 by the authors. Licensee MDPI, Basel, Switzerland. This article is an open access article distributed under the terms and conditions of the Creative Commons Attribution (CC BY) license (<https://creativecommons.org/licenses/by/4.0/>).

1. Introduction

Optical tweezer [1] is a technique that utilizes the radiation pressure of a laser beam to move and control the dynamics of physical objects, such as small particles, atoms, viruses, and other living cells without harming them. This technique is a groundbreaking invention in the field of laser physics and was awarded the Nobel Prize in 2018 for its wide-ranging applications in fields such as biology and physics [2,3]. Along this direction, optical vortices with helical phase beams, which carry the new degree of freedom of orbital angular momentum, have attracted considerable interest in recent years due to their unique physical characteristics, including phase singularity, dark axial intensity distribution and intrinsic orbital angular momentum [4–8]. Differing from the traditional beams, the form of phase singularities in vortex beams during the propagation stage is $\exp(il\varphi)$, where φ represents the azimuthal angle and l represents the TCs; this is an index that indicates the orbital angular momentum carried by each photon in the beams. The rotating phase structure of optical vortices can be employed for manipulating the motion and rotation of particles. Accurate manipulation of microscopic particles can be achieved using optical vortices, such as optical rotation traps [9,10]. Additionally, applications of optical vortices in microscope imaging can provide higher resolution and better demonstration of fine

structures and super-resolution microscope imaging can be accomplished by manipulating the phase and angular momentum of optical vortices [11–13].

In recent decades, various valuable methods based on a range of optical theories have been proposed for generating optical vortices, including spatial light modulators (SLMs) [14], spiral phase plates (SPPs) [15–17], axicons [18,19], devil's vortex lenses [20,21], metasurfaces [22,23] and integrated optical vortex emitters [24,25]. The SZPs proposed by Heckenberg et al. [26] are exemplary for producing optical vortices due to their outstanding advantages such as compact size, light weight and flexibility in design [27]. In particular, SZPs have been widely used as the typical objective lens in the extreme ultraviolet and X-ray regions, whereas SLMs and SPPs struggle to function effectively [28]. Hence, based on the conventional SZPs, in recent years, researchers have investigated modified SZPs to achieve optical vortices with various physical characteristic to satisfy different applications. For current multi-focus research, the application of some aperiodic structures such as Cantor, Fibonacci and Thue–Morse sequences in diffractive elements has attracted considerable attention recently [29–40]. For instance, by combining the Cantor sequence with conventional SZPs, sequence optical vortices with a series of subsidiary foci can be generated at the primary focal plane [41]. Realization of dual principal vortex foci and numerous auxiliary foci along the axial direction is possible with SZPs modified using Thue–Morse and Fibonacci sequences [42–44]. In 2021, the transparent and opaque zones of binary SZPs were rearranged according to the m-bonacci sequence for the generation of the equal-intensity optical vortices on two focused planes. Additionally, composite SZPs consisting of binary phase SZPs are really also an effective way to generate multiple vortices [45]. As mentioned above, these approaches can successfully produce optical vortices with multiple focal planes along the propagation direction. However, the generation of multiple optical vortices with approximately equal intensities remains a challenge.

In this paper, by combining two composite concentric SZPs with the m-bonacci sequence, we propose an effective diffractive optical element termed EMCSZPs to produce multi-focus coaxial optical vortices with equal intensities. The focusing characteristics of such optical elements were calculated and the corresponding demonstration experiment was also carried out and accorded well with our proposal. Differing from the only vortex that appeared at the first primary focal plane of the conventional SZPs, sequential multi-focus vortices can be generated by modulating the incident irradiance with the EMCSZPs and the intensities of these vortices are approximately the same. Furthermore, by appropriately selecting the parameters of the EMCSZPs, we can not only control the distance between two pairs of twin vortices but also the values of TCs of the coaxial optical vortices can be flexibly controlled. The EMCSZPs may open new avenues for improving optical image processing, multi-particle trapping, manipulation and alignment system performance.

2. Design and Method

It is known to us that the conventional SZPs combine radial Hilbert transform with the focusing properties of Fresnel zone plates to generate optical vortices as binary optical elements. The m-bonacci fractional sequence can be composed of m binary elements, starting from $t_{m,0} = \{0\}$ and $t_{m,1} = \{1\}$; let $t_{m,S} = \{t_{m,S-1} t_{m,S-2} \dots t_{m,S-m}\}$ (where $S \geq m$). Beginning with the $m + 1$ element, the elements composing the sequence are formed by concatenating the previous m elements. Figure 1a illustrates the one-dimensional (1D) structural diagram of the Tetranacci sequence ($m = 4$) from order $S = 0$ to $S = 6$.

Conventional SZPs are composed of periodic transparent and opaque annular zones. The fundamental principle of m-bonacci spiral zone plates (MBSZPs) involves adding m-bonacci sequences to the annular zones of SZPs, ensuring that they adhere to the m-bonacci sequence in the radial coordinates. For the conventional SZPs, the transmission function can be expressed as:

$$t(r, \theta) = \exp(i l \theta - \frac{i \pi r^2}{\lambda_f}) \quad (1)$$

where (r, θ) represents polar coordinates, l is the TCs, λ is the wavelength of the incident light and f is the first-order focal length of the SZPs corresponding to the wavelength λ . The SZPs with $l = 1$ are shown in Figure 1b. On this basis, for m-bonacci sequences, we define the transmission function of MBSZPs as:

$$t_{m,S}(r,\theta) = \sum_{n=1}^{N_{m,S+1}} t_{m,s,n} t(r,\theta) \quad (2)$$

where n signifies the number of rings in the zone plate, and S denotes the order of the sequence, $N_{m, S+1}$ represents the sets of elements $t_{m,S}$. EMCSZPs are the combination of two concentric conventional SZPs with different focal lengths; the alternate transparent and opaque zones have been distributed with the specific m-bonacci sequence. Thus, the transmittance of the EMCSZPs can be expressed in terms of a matrix. After binarization, the binary transmittance function of the EMCSZPs can be expressed as $T = t_1 + t_2$, where t_1 and t_2 represent the inner part and outer part transmittances of EMCSZPs, respectively. The respective inner and outer boundaries of the n -th zone of the EMCSZPs with focal length at f_1 are as follows:

$$r_1 = \sqrt{\frac{\lambda f_1(\text{sign}(\theta + \pi(n - 2l - 1)) + 1)(\theta + \pi(n - 2l - 1))}{2\pi}} \quad (3)$$

$$r_2 = \sqrt{\frac{\lambda f_1(\theta + \pi(n - 2l))}{\pi}} \quad (4)$$

where l , λ and f_1 , respectively, represent the TCs, wavelength and focal lengths of the EMCSZPs. Similarly, for zone plates with focal lengths of f_2 , the respective inner and outer boundaries of the n -th zone of the outer zone plates are the same.

Through binary processing, the transmittance function of the EMCSZPs can be expressed as:

$$t(r, \theta) = \begin{cases} 1 & r_1 < r < r_2 \\ 0 & \text{else} \end{cases} \quad (5)$$

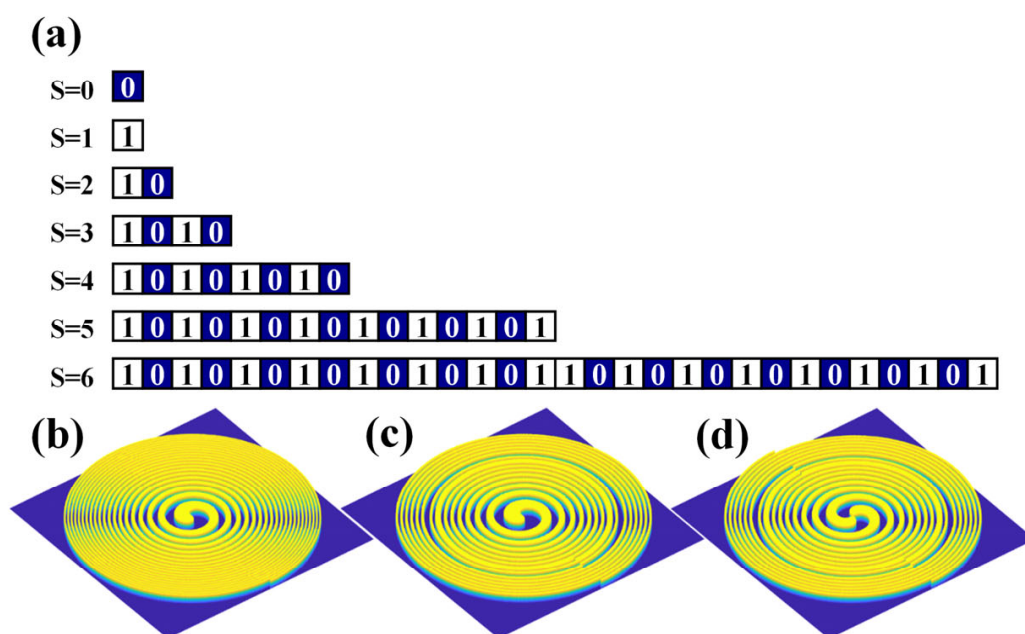


Figure 1. (a) Geometrical construction of the Tetranacci sequence up to order $S = 6$, $m = 4$. The schematic view of SZPs with TCs of (b) $l = 1$. The schematic view of EMCSZPs with TCs of (c) $l = 1$. (d) $l = 2$.

Based on the above discussion, we display the EMCSZPs with different TCs as illustrated in Figure 1c,d. The parameters are set as $m = 4$, $S = 6$ and the grid of sampling points is given as 1080×1080 with pixel size $8 \times 8 \mu\text{m}^2$. In accordance with the above principle, we conducted numerical simulations based on the Fresnel–Kirchhoff diffraction theory and the convolution theorem. Considering a plane wave with a wavelength of λ incident on the diffraction zone plate with a radius of R , the complex amplitude of the diffraction intensity distribution can be expressed as:

$$U(x, y, z) = \frac{\exp(ikz)}{i\lambda z} \int_{-\infty}^{\infty} \int_{-\infty}^{\infty} t_{m,S}(\xi, \eta) \exp\left\{ \frac{ik}{2z} [(x - \xi)^2 + (y - \eta)^2] \right\} d\xi d\eta \quad (6)$$

where $t_{m,S}(\xi, \eta)$ represents the transmittance of the EMCSZPs, and z is the distance between the diffraction zone plane and observation plane. From $I = |U|^2$, the intensity of the beam at any axial position can be determined.

To further address multi-focal properties of the EMCSZPs, as illustrated in Figure 2, we firstly investigate the diffraction properties of the internal and external zones of the EMCSZPs. In the simulation, the parameters are wavelength $\lambda = 632.8 \text{ nm}$, focal length $f_1 = 260 \text{ mm}$, $f_2 = 310 \text{ mm}$ and TC $l = 1$. As we know that if we rearrange the transparent and opaque zones of the conventional SZPs in accordance with the Tetranacci sequence, the optical vortex at the first primary focal plane will split into a pair vortices with equal intensities. Along this line, we proposed the composite zone plate termed EMCSZPs for generating optical vortices with equal intensities and multi-focus characteristics by nesting two concentric conventional SZPs with different focal lengths together. Just as mentioned, because the transparent and opaque zones have been rearranged according to the typical Tetranacci sequence, this new diffractive optical element would satisfy our physical prediction. To verify the theoretical design, we calculated focusing properties of the inner zones and outer zones of the EMCSZPs along the propagation direction, respectively. In the simulation, as displayed in Figure 2a, we define the first 29 rings as the inner parts and the focal length is $f_1 = 260 \text{ mm}$. Meanwhile, we can see from Figure 2c that the last 30 rings with a focal length of $f_2 = 310 \text{ mm}$ consist of the outer parts. From the comparison, it can be concluded from Figure 2b,d that both the inner zones and the outer zones can produce optical vortices with twin axial foci. Nevertheless, considering the inherent phase difference, the hollow beams are focused at different positions. The findings may provide additional possibilities for optical research.

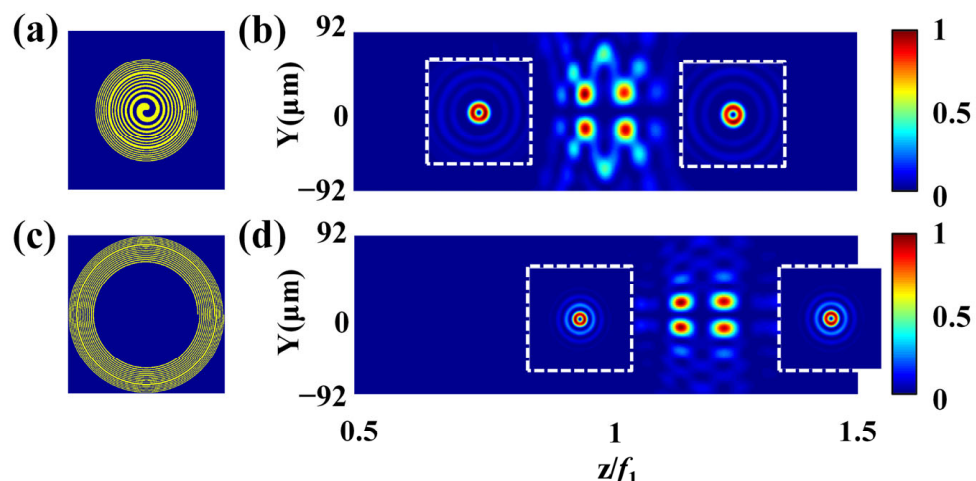


Figure 2. (a) The inner zone plates for the first 29 rings of EMCSZPs. (b) Axial and transverse irradiance profiles of inner zone plates. (c) The outer zone plates and (d) axial and transverse irradiance profiles for the following 30 rings of EMCSZPs.

3. Focusing Properties of the EMCSZPs

To emphasize the focusing characteristics of the EMCSZPs, as illustrated in Figure 3, we present the focusing performance of conventional SZPs and EMCSZPs for comparison under the same circumstance. In the calculation, the incident wavelength $\lambda = 632.8$ nm and the m-bonacci sequence parameters are $m = 4$ and $S = 8$, which are also adopted in our experiment for rigorous verification. From Figure 3a,b, we can see that both the SZPs and the EMCSZPs can generate hollow beams along the propagation direction. However, different from other cases in which there is only one vortex, which appears at the first primary focal plane for the conventional SZPs, the EMCSZPs can produce four optical vortices. Considering that the optical vortex carrying orbital angular momentum can transfer energy to other physical objects, the focusing performance of EMCSZPs with $l = 2$ are further discussed in Figure 3c. From the transverse intensity profiles, one can identify that when the incident light is regulated by EMCSZPs with $l = 2$, larger diameter hollow beams can be produced at the first primary focal plane. The diameters of the focused vortices with $l = 1$ are 66 μm , 62 μm , 51 μm and 55 μm , respectively, and the diameters with $l = 2$ are 91 μm , 97 μm , 72 μm and 77 μm , respectively. In addition, it can be found from the intensity distribution curves in Figure 3d,e that the four foci of the constructed EMCSZPs have the identical intensity peak approximately.

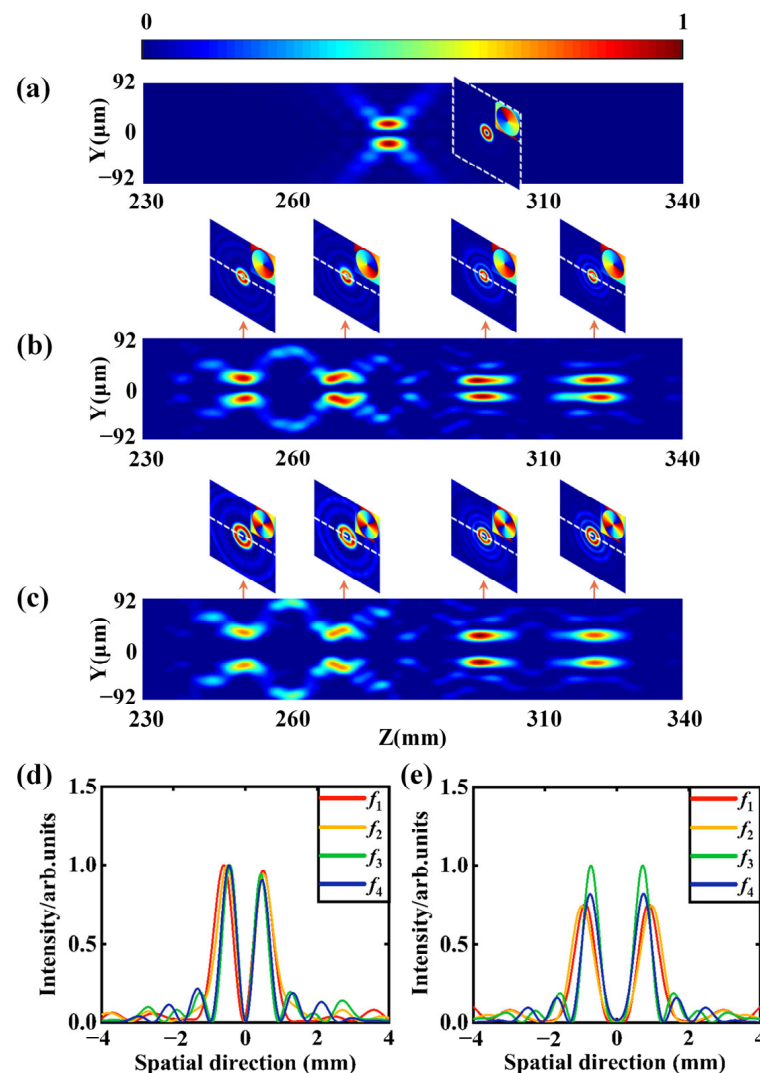


Figure 3. Far-field diffraction intensity distribution on the y - z ($x = 0$) plane and transverse irradiance and phase profiles on the x - y ($z = 0$) plane: (a) conventional SZPs, (b) EMCSZPs of $l = 1$, (c) EMCSZPs of $l = 2$. (d,e) The normalized vortex intensities along the dashed lines in (b,c).

As mentioned above, considering the proposed EMCSZPs are composed by two concentric conventional SZPs with different focal lengths according to the m-bonacci sequence, we can effectively adjust the axial distribution of the phase singularity by modifying the parameters of the inner zones and outer zones. It is known to us that both the inner parts and the outer parts of the EMCSZPs can produce one pair of equal intensity vortices. If the fractal sequence parameters m and S remain the same as those in the calculation in Figure 3, it can be clearly deduced from Figure 4a–c that when the focal length difference between the inner zones and outer zones is increased from 50 mm to 70 mm, the distance between the two pairs of focused vortices is similarly increased from 48.62 mm to 69.08 mm. The distances between the first focal plane z_1 and second focal plane z_2 produced by the inner zones, and the third focal plane z_3 and fourth focal plane z_4 produced by the outer zones are still unchangeable. It is worth noting that the ratio of the transverse distances between the first and second vortex, and the third and fourth vortex locations consistently satisfies $\tau = z_2/z_1 = z_4/z_3 \approx 1.07$, approximately equivalent to the golden ratio of 1.078 in the m-bonacci sequence with $m = 4$ [46,47]. To satisfy the physical design for generating multi-focus along the propagation direction, the focal length of the inner parts needs to be smaller and thus the quality of the vortices near f_1 is slightly affected.

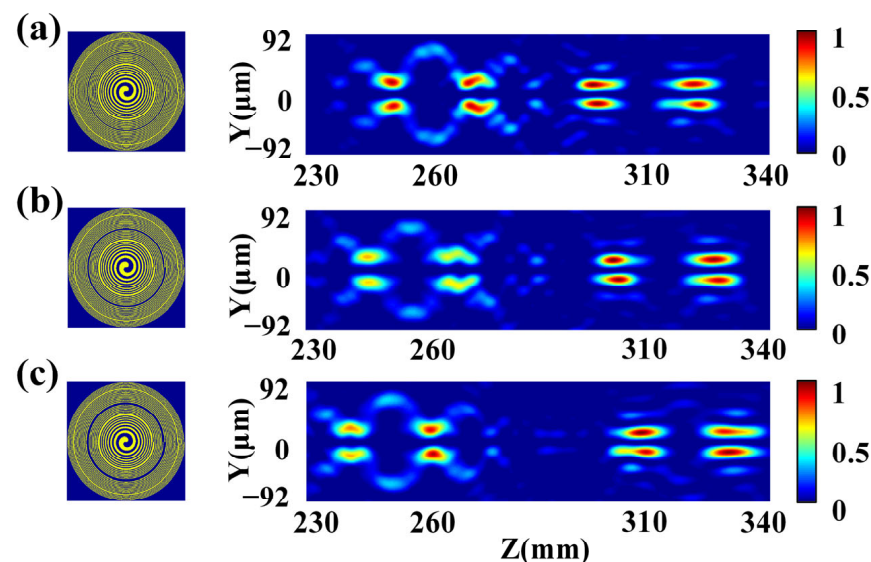


Figure 4. EMCSZP schematic diagram for changing the focal lengths of inner and outer zone plates and EMCSZP axial irradiation diagram. We set the focal length of the inner zone plates as f_1 and the focal length of the outer zone plates as f_2 . (a) $f_1 = 260$ mm, $f_2 = 310$ mm, (b) $f_1 = 255$ mm, $f_2 = 315$ mm, (c) $f_1 = 250$ mm, $f_2 = 320$ mm.

However, considering the strong penetration of X-rays, the dark region in the banded plate, as shown in Figure 1a, is partially transparent due to the strong penetrability of X-rays. In practice, the absorbing material is typically a high-Z foil, such as gold foil. Therefore, the binary transmittance $t_{m,S}(r,\theta)$ of EMCSZPs in Equation (5) can be replaced by $t'_{m,S}(r,\theta)$, which can be written as:

$$t'(r,\theta) = \begin{cases} 1 & \text{the transparent zones} \\ \exp[-kd(\beta + i\delta)] & \text{the opaque zones} \end{cases} \quad (7)$$

where the parameter d is the thickness of the gold foil, and δ and β are the X-ray optical constants of gold. These constants vary with the incident wavelength. The chosen values for these parameters are $d = 500$ nm, $\delta = 6.7382 \times 10^{-2}$ and $\beta = 9.7501 \times 10^{-3}$.

By combining Equations (6) and (7), we can conclude that the performance of gold foil EMCSZPs in generating multiple foci is comparable to that of ideal ones. From Figure 5a,b, it can be observed that even when considering the additional phase shift introduced by

X-rays, the ability of EMCSZPs to generate multi-focus vortices with equal intensity is not affected.

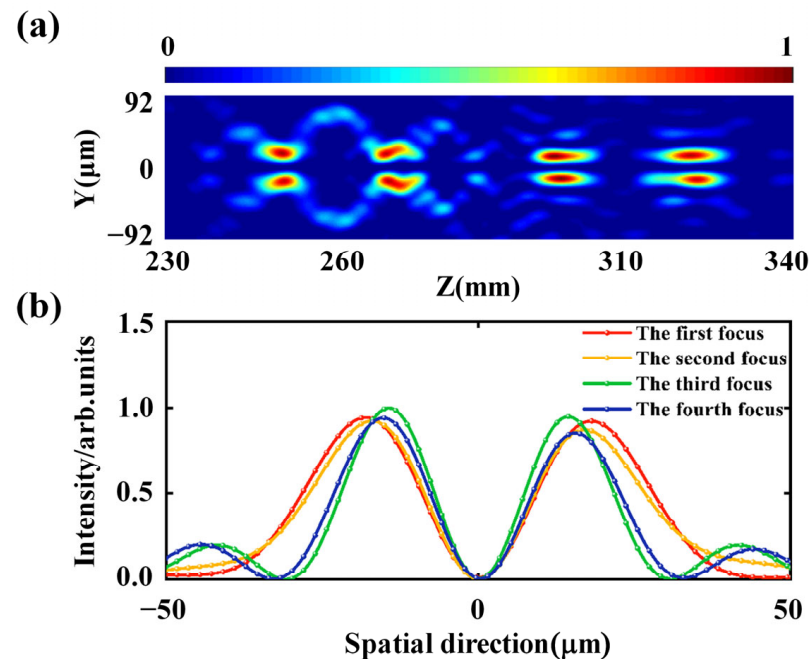


Figure 5. (a) The calculated axial irradiance EMCSZPs in X-ray region. (b) Corresponding intensity profiles along the z - x plane ($y = 0$).

4. Experimental Results

To examine the feasibility of the proposed EMCSZPs, we perform the demonstration experiment as illustrated in Figure 6a. In this typical configuration, a He-Ne laser beam with a wavelength of 632 nm was first extended and collimated by lenses L1 and L2, then impinging on a polarizing beam splitter (PBS), one beam is projected onto the SLM and the other is loaded onto the charge-coupled device (CCD), and finally it is irradiated onto the EMCSZPs. The intensity distributions of the reflected beam at different distances from the EMCSZPs were measured with the help of a sliding guide using a CCD (DCU-224-M, 1280×1024 pixels, $2.2 \mu\text{m} \times 2.2 \mu\text{m}/\text{pixel}$). Considering the flexibility of the SLM, we experimentally fabricated the holograms of EMCSZPs with a reflective-type SLM (HOLOEYE, 1920×1080 pixels, $8 \mu\text{m} \times 8 \mu\text{m}/\text{pixel}$) and chose the same parameters, $f_1 = 260 \text{ mm}$, $f_2 = 310 \text{ mm}$, $m = 4$ and $S = 8$, for the EMCSZPs as for the simulations in Figure 3. Specifically, in order to better demonstrate the transmission characteristics of the modulated optical field, we utilized a sliding rail to record diffraction patterns of 500 images. This process allowed us to reconstruct the overall axial irradiance within the focused vortex range. We recorded the axial irradiance intensities with TCs of $l = 1$ and $l = 2$, as well as the corresponding intensity distribution of each focused vortex in the x - y plane.

The reconstructed axial irradiance and the lateral intensity distribution of each vortex focus are shown in Figure 6b–e. It can be seen that EMCSZPs with $l = 1$ and $l = 2$ can indeed generate four focused vortices with approximately equal intensities along the optical axis, which is consistent with our calculation as presented in Figure 3b,d. Additionally, to precisely accurately measure the value of orbital angular momentum carried by the four equally intense vortices, we perform additional experiment on focused vortices with different TCs based on interferometric measurement methods. By interfering with plane waves and modulated vortex light in different focal planes, we clearly obtain the fork stripes characterized by optical vortices. As illustrated in Figure 6b,d, the upper right corner represents the interference pattern corresponding to each focal vortex. Based on the difference between the number of fringes above and below the interferogram, the orbital

angular momentum of the optical vortices produced by EMCSZPs can be identified. From the interference patterns of the vortex beam with a plane wave incident light at different focal planes, we can infer that the EMCSZPs can generate four optical vortices with equal intensities and the same TCs, exhibiting characteristics superior to those of the simulation in Figure 3b,c. In addition, the ratio between the relative diameters of each pair of focused vortices is $z_2/z_1 = z_4/z_3 \approx 1.07$, and this result matches well with the predicted value $\tau_4 = 1.078$ within the error range. Noticeably, by adjusting the parameters of EMCSZPs, it is also possible to generate optical vortices with different TCs. These features endow the EMCSZPs with an extensive application in various fields such as three-dimensional optical operations and multiple particle manipulation.

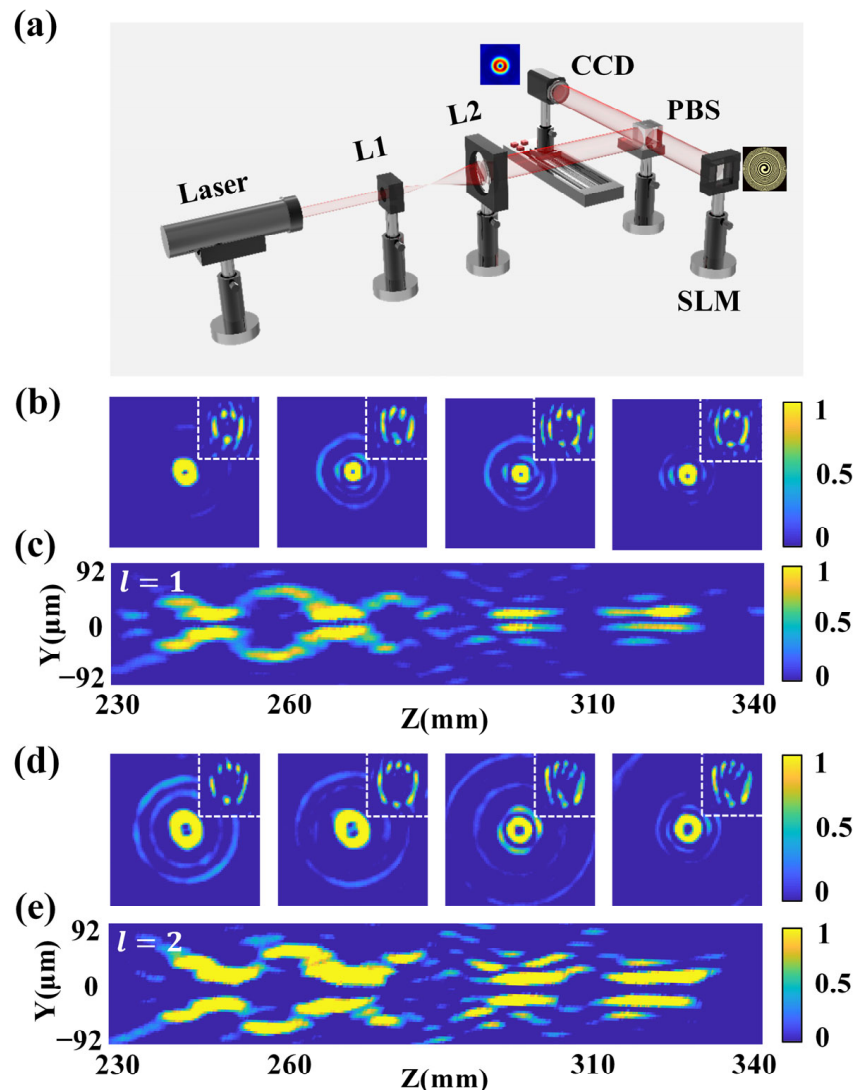


Figure 6. Experimental results of the EMCSZPs. (a) Schematic diagram of experimental setup. (b) The transverse irradiance and phase profiles on the x - y plane of $l = 1$. (c) The reconstructed axial irradiance results for $l = 1$ on the y - z plane ($x = 0$). (d) The transverse irradiance and phase profiles and (e) the reconstructed axial irradiance of $l = 2$.

5. Discussion

Due to the rapid development and wide application of optical vortices, how to efficiently generate multiple vortices with uniform intensity has become a prominent subject of discussion and research. In recent years, composite spiral zone plates and the application of some aperiodic structures in diffractive elements have been used to generate multiple foci along the axis. Nevertheless, currently, it is still a challenge to produce coaxial optical

vortices with multi-foci and equal intensity simultaneously in one step. To overcome these shortcomings, in our physical design, we proposed the effective methodology terms as EM-CSZPs by combining two concentric SZPs with different focal lengths together and a radial structure based on the Fibonacci sequence was also added. Compared with the composite SZPs consisting of binary phase SZPs, the technique based on the Fibonacci sequence may split each main focus into further doubling of focal spots, the intensity of which will be uniformly distributed. The typical focusing performance may offer a possible alternative in the fields of optical tweezer and trap techniques by capturing multiple particles at the same time on the focal planes with equal intensities. As for the fields of laser micro-machining, the multiple vortices are evenly distributed at different focal planes, and therefore they will offer higher precision in the process of cutting materials with different thickness. In addition, the multi-focus vortices may provide an extensive application in the fields of biomedical imaging and super-resolution 3D imaging by simultaneously obtaining the depth information of target objects at different focal planes.

Specifically, it is worth noting that, to satisfy the physical design for generating multi-focus along the propagation direction, the focal length of the inner parts needs to be smaller and then the effective irradiation dimension will unavoidably be smaller. Resultantly, the quality of the vortices near f_1 is slightly affected. We know that dividing the aperture into annular sub-apertures is not the only possible solution, and several diffractive lenses can be written by spatial multiplexing in a random scheme without loss of resolution due to smaller apertures [48,49]. In addition, by introducing the neural network algorithms, the axial distributions of the ZPs can be improved and the undesired higher diffraction foci can be successfully suppressed [50]. In future endeavors, we will dedicate work to further optimizing the focusing performance of our proposal by exploiting particular algorithms.

6. Conclusions

In summary, we propose a diffractive optical element termed EMCSZPs for generating multiple coaxial optical vortices with equal intensity along the propagation direction. Based on the Fresnel–Kirchhoff theory and the convolution theorem, the focusing performance was comprehensively investigated. Differing from the single optical vortex that appeared at the first primary focal plane as that of the conventional SZP, EMCSZPs have superior performance in terms of producing optical vortices with multi-focus and equal intensity. Interestingly, by optimizing the parameters of the EMCSZPs, the axial positions and TCs of the multi-focus vortices can be further flexibly controlled. The corresponding experimental verification was also performed to verify our physical design. In addition, considering the binarization characteristics, this optical element can also be extended to the X-ray region. The results indicate that this new component can be applied to trap particles with an equal trapping force at multi-planes, and offers broad applications in areas such as ultra-high-resolution imaging, lithography, optical trapping and optical communication.

Author Contributions: Investigation, methodology, writing, H.Z.; simulation, writing, J.L. and C.Z.; review & editing, L.W.; visualization, Q.F. and S.W.; supervision, C.W., Y.T. and J.X.; funding acquisition, H.Z., C.Z. and L.C. All authors have read and agreed to the published version of the manuscript.

Funding: This work was funded by the National Natural Science Foundation of China (Grant No. 12174350, H.Z.); Excellent Youth Foundation of He'nan Scientific Committee (Grant No. 232300421076, H.Z.); China Postdoctoral Science Foundation (Grant Nos. 2023TQ0296 and GZC20232389, C.Z.); Financial Support for Outstanding Talents Training Fund in Shenzhen (Grant No. 202101, L.C.); Financial Assistance Program for Newly Introduced High-end Talents of Shenzhen University of Technology (Grant No. 20200206, L.C.).

Data Availability Statement: The data underlying the results presented in this paper are not publicly available at this time but may be obtained from the authors upon reasonable request.

Conflicts of Interest: The authors declare no conflicts of interest.

References

- Ashkin, A.; Dziedzic, J.M. Optical trapping and manipulation of viruses and bacteria. *Science* **1987**, *235*, 1517–1520. [CrossRef] [PubMed]
- The Nobel Prize in Physics 2018. Nobel Prize Outreach AB 2022. 2022. Available online: <https://www.nobelprize.org/prizes/physics/2018/summary/> (accessed on 1 August 2023).
- Zang, H.; Miao, Z.; Wang, M.; Fan, Q.; Wei, L.; Wang, C.; Zhou, W.; Hua, Y.; Cao, L.; Xue, X.; et al. Generation of single-focus phase singularity by the annulus-quadrangle-element coded binary square spiral zone plates. *Sci. China Phys. Mech. Astron.* **2022**, *65*, 294212. [CrossRef]
- Ni, J.; Huang, C.; Zhou, L.; Gu, M.; Song, Q.; Kivshar, Y.; Qiu, C. Multidimensional phase singularities in nanophotonics. *Science* **2021**, *374*, eabj0039. [CrossRef] [PubMed]
- Verbeeck, J.; Tian, H.; Schattschneider, P. Production and application of electron vortex beams. *Nature* **2010**, *467*, 301–304. [CrossRef] [PubMed]
- Liu, M.; Zhao, C.; Zeng, Y.; Chen, Y.; Zhao, C.; Qiu, C. Evolution and nonreciprocity of loss-induced topological phase singularity pairs. *Phys. Rev. Lett.* **2021**, *127*, 266101. [CrossRef]
- Shen, Y.; Wang, X.; Xie, Z.; Min, C.; Fu, X.; Liu, Q.; Gong, M.; Yuan, X. Optical vortices 30 years on: OAM manipulation from topological charge to multiple singularities. *Light Sci. Appl.* **2019**, *8*, 90. [CrossRef] [PubMed]
- Bliokh, K.Y. Orbital angular momentum of optical, acoustic, and quantum-mechanical spatiotemporal vortex pulses. *Phys. Rev. A* **2023**, *107*, L031501. [CrossRef]
- Min, C.; Shen, Z.; Shen, J.; Zhang, Y.; Fang, H.; Yuan, G.; Du, L.; Zhu, S.; Lei, T.; Yuan, X. Focused plasmonic trapping of metallic particles. *Nat. Commun.* **2013**, *4*, 2891. [CrossRef] [PubMed]
- Xia, T.; Cheng, S.; Tao, S. The generalized mean zone plate. *Laser Phys.* **2018**, *28*, 066201. [CrossRef]
- Pascucci, M.; Tessier, G.; Emiliani, V.; Guillou, M. Superresolution imaging of optical vortices in a speckle pattern. *Phys. Rev. Lett.* **2016**, *116*, 093904. [CrossRef]
- Gao, N.; Xie, C.; Li, C.; Jin, C.; Liu, M. Square optical vortices generated by binary spiral zone plates. *Appl. Phys. Lett.* **2011**, *98*, 151106. [CrossRef]
- Zang, H.; Wang, B.; Zheng, C.; Wei, L.; Fan, Q.; Wang, S.; Yang, Z.; Zhou, W.; Cao, L.; Guo, H. Performance analysis of single-focus phase singularity based on elliptical reflective annulus quadrangle-element coded spiral zone plates. *Chin. Phys. B* **2023**, *33*, 014209. [CrossRef]
- Yang, Y.; Forbes, A.; Cao, L. A review of liquid crystal spatial light modulators: Devices and applications. *Opto-Electron. Sci.* **2023**, *2*, 230026-1–230026-29. [CrossRef]
- Khonina, S.N.; Ustinov, A.V.; Logachev, V.I.; Porfirev, A.P. Properties of vortex light fields generated by generalized spiral phase plates. *Phys. Rev. A* **2020**, *101*, 043829. [CrossRef]
- Nassiri, M.G.; Brasselet, E. Multispectral management of the photon orbital angular momentum. *Phys. Rev. Lett.* **2018**, *121*, 213901. [CrossRef] [PubMed]
- Géneaux, R.; Camper, A.; Augste, T.; Gobert, O.; Caillat, J.; Taïeb, R.; Ruchon, T. Synthesis and characterization of attosecond light vortices in the extreme ultraviolet. *Nat. Commun.* **2016**, *7*, 12583. [CrossRef]
- Rego, L.; San Román, J.; Picón, A.; Plaja, L.; Hernández-García, C. Nonperturbative twist in the generation of extreme-ultraviolet vortex beams. *Phys. Rev. Lett.* **2016**, *117*, 163202. [CrossRef]
- Aleksanyan, A.; Brasselet, E. Spin-orbit photonic interaction engineering of Bessel beams. *Optica* **2016**, *3*, 167–174. [CrossRef]
- Pu, J.; Jones, P.H. Devil’s lens optical tweezers. *Opt. Express* **2015**, *23*, 8190–8199. [CrossRef]
- Singh, H.; Yadav, A.K.; Vashisth, S.; Singh, K. Optical image encryption using devil’s vortex toroidal lens in the Fresnel transform domain. *Int. J. Opt.* **2015**, *2015*, 926135. [CrossRef]
- Zang, H.; Zhou, X.; Yang, Z.; Yu, Q.; Zheng, C.; Yao, J. Polarization multiplexed multifunctional metasurface for generating longitudinally evolving vector vortex beams. *Phys. Lett. A* **2024**, *497*, 129336. [CrossRef]
- Zheng, C.; Liu, J.; Li, H.; Wang, M.; Zang, H.; Zhang, Y.; Yao, J. Terahertz metasurface polarization detection employing vortex pattern recognition. *Photonics Res.* **2023**, *11*, 2256–2263. [CrossRef]
- Karabchevsky, A. On-chip optical vortex-based nanophotonic detectors. *Light Sci. Appl.* **2020**, *9*, 115. [CrossRef] [PubMed]
- White, A.D.; Su, L.; Shahar, D.I.; Yang, K.Y.; Ahn, G.H.; Skarda, J.L.; Ramachandran, S.; Vučović, J. Inverse design of optical vortex beam emitters. *ACS Photonics* **2022**, *10*, 803–807. [CrossRef]
- Heckenberg, N.R.; McDuff, R.; Smith, C.P.; White, A.G. Generation of optical phase singularities by computer-generated holograms. *Opt. Lett.* **1992**, *17*, 221–223. [CrossRef] [PubMed]
- Tsukamoto, Y.; Yoshida, H.; Ozaki, M. Generation of a focused optical vortex beam using a liquid crystal spiral zone plate. *Opt. Express* **2022**, *30*, 8667–8675. [CrossRef]
- Yi, S.; Mu, B.; Wang, X.; Zhang, Z.; Zhu, J.; Wang, Z.; He, P.; Cao, Z.; Dong, J.; Liu, S.; et al. Large-field high-resolution Kirkpatrick–Baez amélioré–Kirkpatrick–Baez mixed microscope for multi-keV time-resolved X-ray imaging diagnostics of laser plasma. *Opt. Eng.* **2014**, *53*, 053114. [CrossRef]
- Gao, N.; Zhang, Y.; Xie, C. Circular Fibonacci gratings. *Appl. Opt.* **2011**, *50*, G142–G148. [CrossRef] [PubMed]
- Monsoriu, J.A.; Calatayud, A.; Remón, L.; Furlan, W.D.; Saavedra, G.; Andrés, P. Bifocal Fibonacci diffractive lenses. *IEEE Photonics J.* **2013**, *5*, 3400106. [CrossRef]

31. Calatayud, A.; Ferrando, V.; Remón, L.; Furlan, W.D.; Monsoriu, J.A. Twin axial vortices generated by Fibonacci lenses. *Opt. Express* **2013**, *21*, 10234–10239. [[CrossRef](#)]
32. Teng, S.; Wang, J.; Li, F.; Zhang, W. Talbot image of two-dimensional fractal grating. *Opt. Commun.* **2014**, *315*, 103–107. [[CrossRef](#)]
33. Verma, R.; Banerjee, V.; Senthilkumaran, P. Fractal signatures in the aperiodic Fibonacci grating. *Opt. Lett.* **2014**, *39*, 2557–2560. [[CrossRef](#)] [[PubMed](#)]
34. Verma, R.; Sharma, M.K.; Senthilkumaran, P.; Banerjee, V. Analysis of Fibonacci gratings and their diffraction patterns. *J. Opt. Soc. Am. A* **2014**, *31*, 1473–1480. [[CrossRef](#)] [[PubMed](#)]
35. Ferrando, V.; Calatayud, A.; Andrés, P.; Torroba, R.; Furlan, W.D.; Monsoriu, J.A. Imaging properties of Kinoform Fibonacci lenses. *IEEE Photonics J.* **2014**, *6*, 6500106. [[CrossRef](#)]
36. Monsoriu, J.A.; Giménez, M.H.; Furlan, W.D.; Barreiro, J.C.; Saavedra, G. Diffraction by m-bonacci gratings. *Eur. J. Phys.* **2015**, *36*, 065005. [[CrossRef](#)]
37. Machado, F.; Ferrando, V.; Furlan, W.D.; Monsoriu, J.A. Diffractive m-bonacci lenses. *Opt. Express* **2017**, *25*, 8267–8273. [[CrossRef](#)] [[PubMed](#)]
38. Pérez-López, S.; Fuster, J.M.; Candelas, P. M-Bonacci zone plates for ultrasound focusing. *Sensors* **2019**, *19*, 4313. [[CrossRef](#)] [[PubMed](#)]
39. Perez-Lopez, S.; Fuster, J.M.; Candelas, P.; Rubio, C. Fractal lenses based on Cantor binary sequences for ultrasound focusing applications. *Ultrasonics* **2019**, *99*, 105967. [[CrossRef](#)] [[PubMed](#)]
40. Xia, T.; Cheng, S.; Yu, W.; Tao, S. Tailorable polygon-like beams generated by modified spiral petal-like zone plates. *Results Phys.* **2021**, *21*, 103823. [[CrossRef](#)]
41. Ferrando, V.; Calatayud, A.; Giménez, F.; Furlan, W.D.; Monsoriu, J.A. Cantor dust zone plates. *Opt. Express* **2013**, *21*, 2701–2706. [[CrossRef](#)]
42. Ma, W.; Tao, S.; Cheng, S. Composite Thue-Morse zone plates. *Opt. Express* **2016**, *24*, 12740–12747. [[CrossRef](#)]
43. Ferrando, V.; Giménez, F.; Furlan, W.D.; Monsoriu, J.A. Bifractal focusing and imaging properties of Thue-Morse Zone Plates. *Opt. Express* **2015**, *23*, 19846–19853. [[CrossRef](#)] [[PubMed](#)]
44. Cheng, S.; Liu, M.; Xia, T.; Tao, S. Fibonacci-like zone plate. *Laser Phys.* **2018**, *28*, 066203. [[CrossRef](#)]
45. Liu, J.; Jiang, P.; Yang, H.; Qin, Y.; Zheng, Y. Multi-focus composite spiral zone plate to generate focused vortices with the comparable intensity based on genetic algorithm. *Opt. Express* **2023**, *31*, 35363–35376. [[CrossRef](#)]
46. Waddill, M.E. The Tetranacci sequence and generalizations. *Fibonacci Q.* **1992**, *30*, 9–20.
47. Sharma, K.K.; Panwar, V. On Tetranacci Functions and Tetranacci Numbers. *Int. J. Math. Comput. Sci.* **2020**, *15*, 923–932.
48. Iemmi, C.; Campos, J.; Escalera, J.C.; López-Coronado, O.; Gimeno, R.; Yzuel, M.J. Depth of focus increase by multiplexing programmable diffractive lenses. *Opt. Express* **2006**, *14*, 10207–10219. [[CrossRef](#)] [[PubMed](#)]
49. Vergara, M.; Iemmi, C. Multiple quasi-perfect vector vortex beams with arbitrary 3D position on focus. *Appl. Opt.* **2022**, *61*, 5926–5933. [[CrossRef](#)]
50. Zang, H.; Wang, Y.; Zheng, C.; Zhou, W.; Wei, L.; Cao, L.; Fan, Q. Generalized binary spiral zone plates with a single focus obtained by feedforward neural network. *Opt. Express* **2023**, *31*, 30486–30494. [[CrossRef](#)]

Disclaimer/Publisher’s Note: The statements, opinions and data contained in all publications are solely those of the individual author(s) and contributor(s) and not of MDPI and/or the editor(s). MDPI and/or the editor(s) disclaim responsibility for any injury to people or property resulting from any ideas, methods, instructions or products referred to in the content.